NEW DIFFRACTION DATA

Crystal structure of palovarotene, $C_{27}H_{30}N_2O_2$

James A. Kaduk[1,2] (iD), Anja Dosen[3] (iD) and Tom Blanton[3] (iD)

[1]Department of Chemistry, Illinois Institute of Technology, 3101 South Dearborn Street, Chicago, IL 60616, USA
[2]Department of Physics, North Central College, 131 South Loomis Street, Naperville, IL 60540, USA
[3]International Centre for Diffraction Data (ICDD), 12 Campus Boulevard, Newtown Square, PA 19073-3273, USA

Abstract: The crystal structure of palovarotene has been solved and refined using synchrotron X-ray powder diffraction data and optimized using density functional theory techniques. Palovarotene crystallizes in the space group *P-1* (#2) with a = 10.2914(4), b = 11.8318(7), c = 11.9210(5) Å, α = 66.2327(11), β = 82.5032(9), γ = 65.3772(9)°, V = 1,206.442(28) Å^3, and Z = 2 at 298 K. The crystal structure consists of chains of O–H⋯N hydrogen-bonded palovarotene molecules along the <0,−1,1> axis; the graph set is *C1,1(14)*. The powder pattern has been submitted to the International Centre for Diffraction Data® for inclusion in the Powder Diffraction File™ (PDF®).

Key words: palovarotene, Sohonos, crystal structure, Rietveld refinement, density functional theory

I. INTRODUCTION

Palovarotene (marketed under the trade name Sohonos) is administered orally for treating and reducing connective tissue turning into bone diseases. This phenomenon, including heterotopic ossification (bone grows outside of the skeleton in soft tissue) and fibrodysplasia ossifans progressive (connective tissue turns into bone), is most often associated with trauma or surgery to hips and legs (Leslie, 2024). The systematic name (CAS Registry No. 410528-02-8) is 4-[(E)-2-[5,5,8,8-tetra-methyl-3-(pyrazol-1-ylmethyl)-6,7-dihydronaphthalen-2-yl] ethenyl]benzoic acid. A two-dimensional molecular diagram of palovarotene is shown in Figure 1.

We are unaware of any published X-ray powder diffraction data for palovarotene. This work was carried out as part of a project (Kaduk et al., 2014) to determine the crystal structures of large-volume commercial pharmaceuticals and include high-quality powder diffraction data for them in the Powder Diffraction File™ (Kabekkodu et al., 2024).

II. EXPERIMENTAL

Palovarotene was a commercial reagent, purchased from TargetMol (Batch #130336) and was used as received. The white powder was packed into a 0.5-mm-diameter Kapton capillary and rotated during the measurement at ~2 Hz. The powder pattern was measured at 298(1) K at the BXDS-WLE Wiggler Low Energy Beamline (Leontowich et al., 2021) of the Brockhouse X-ray Diffraction and Scattering Sector of the Canadian Light Source using a wavelength of 0.819563(2) Å

(15.1 keV) from 1.6 to 75.0° 2θ with a step size of 0.0025° and a collection time of 3 minutes. The high-resolution powder diffraction data were collected using eight Dectris Mythen2 X series 1K linear strip detectors. NIST SRM 660b LaB$_6$ (Black et al., 2011) was used to calibrate the instrument and refine the monochromatic wavelength used in the experiment.

The pattern was indexed with N-TREOR (Altomare et al., 2013) on a primitive triclinic unit cell with a = 10.29713, b = 11.83345, c = 11.92548 Å, α = 66.277, β = 82.512, γ = 65.386°, V = 1,208.2 Å^3, and Z = 2. The space group was assumed to be *P-1*, which was confirmed by the successful solution and refinement of the structure. A reduced cell search of the Cambridge Structural Database (Groom et al., 2016) yielded no hits.
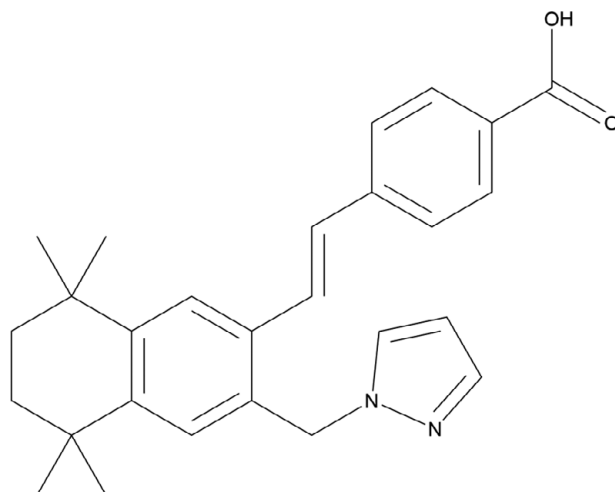

Figure 1. The two-dimensional structure of palovarotene.

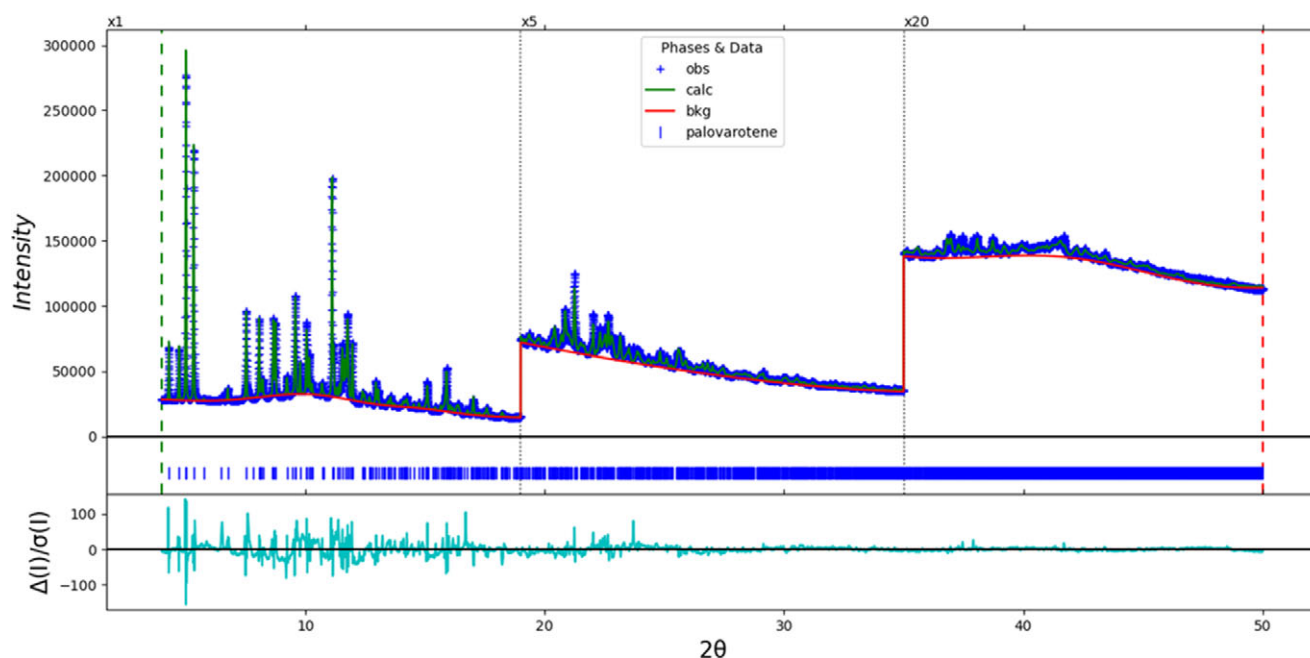Corresponding author: James Kaduk; Email: kaduk@polycrystallography.com

Figure 2. The Rietveld plot for palovarotene. The blue crosses represent the observed data points, and the green line represents the calculated pattern. The cyan curve indicates the normalized error plot, and the red line indicates the background curve. The vertical scale has been multiplied by a factor of 5× for $2\theta > 19.0°$ and by a factor of 20× for $2\theta > 35.0°$.

The palovarotene molecule was downloaded from PubChem (Kim et al., 2023) as Conformer3D_COMPOUND_CID_ 10295295.sdf. It was converted to a *.mol2 file using Mercury (Macrae et al., 2020), and to a Fenske-Hall Z-matrix file using OpenBabel (O'Boyle et al., 2011). The crystal structure was solved using Monte Carlo-simulated annealing techniques as implemented in FOX (Favre-Nicolin and Černý, 2002), using $(\sin\theta/\lambda)_{max} = 0.26$ Å^{-1}.

The best solution refined to $R_{wp} = 0.0373$, but was chemically unreasonable. There was a void, surrounded by hydrophilic groups (the carboxylic acid and pyrazole ring), but no hydrogen bonds. The visual examination of the structure revealed that, if both the pyrazole ring and the carboxylic acid group were rotated by ~180°, the "free" N and hydroxyl group would become close enough to form an O–H⋯N hydrogen bond. These manipulations were carried out using Materials Studio (Dassault Systèmes, 2023). Both the original and "flipped" structures were optimized using VASP (Kresse and Furthmüller, 1996). The "flipped" structure was 14.6 kcal/mol lower in energy than the original, so the final refinement was carried out using the flipped structure.

Rietveld refinement was carried out with GSAS-II (Toby and Von Dreele, 2013). Only the 4.0–50.0° portion of the pattern was included in the refinements ($d_{min} = 0.969$ Å). All non-H-bond distances and angles were subjected to restraints, based on a Mercury/Mogul Geometry Check (Bruno et al., 2004; Sykes et al., 2011). The Mogul average and standard deviation for each quantity were used as the restraint parameters. The aromatic rings were restrained to be planar. The restraints contributed 4.3% to the overall χ^2. The hydrogen atoms were included in calculated positions, which were recalculated during the refinement using Materials Studio (Dassault Systèmes, 2023). The U_{iso} of the heavy atoms were grouped by chemical similarity. The U_{iso} for the H atoms were fixed at 1.3× the U_{iso} of the heavy atoms to which they are attached. The peak profiles were described using the generalized microstrain model (Stephens,

1999). The background was modeled using a three-term shifted Chebyshev polynomial, with broad peaks at 10.21, 14.76, and 41.72° to model the scattering from the Kapton capillary and any amorphous component. An O atom (water molecule) was placed in the void, but its occupancy was refined to only 0.01, and it was deleted from the model.

The final refinement of 130 variables using 18,401 observations and 88 restraints yielded the residual $R_{wp} = 0.0294$. The largest peak (0.78 Å from C16) and hole (1.62 Å from H52) in the difference Fourier map were 0.32(8) and −0.33 (8) eÅ^{-3}, respectively. The final Rietveld plot is shown in Figure 2. The largest features in the normalized error plot are in the shapes and positions of some of the low-angle peaks, as well as at peaks of an unidentified trace impurity.

The crystal structure of palovarotene was optimized (fixed experimental unit cell) with density functional techniques using VASP (Kresse and Furthmüller, 1996) through the MedeA graphical interface (Materials Design, 2024). The
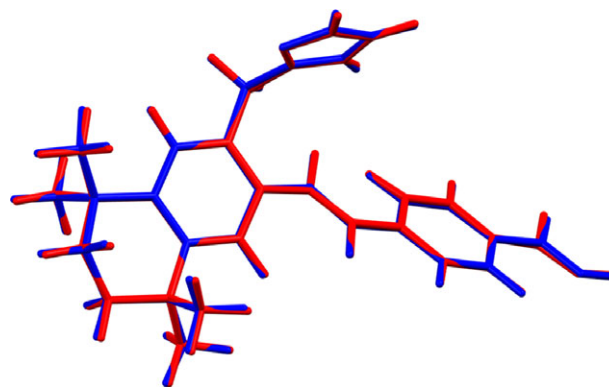

Figure 3. Comparison of the Rietveld-refined (red) and VASP-optimized (blue) structures of palovarotene. The root-mean-square Cartesian displacement is 0.091 Å. Image generated using Mercury (Macrae et al., 2020).
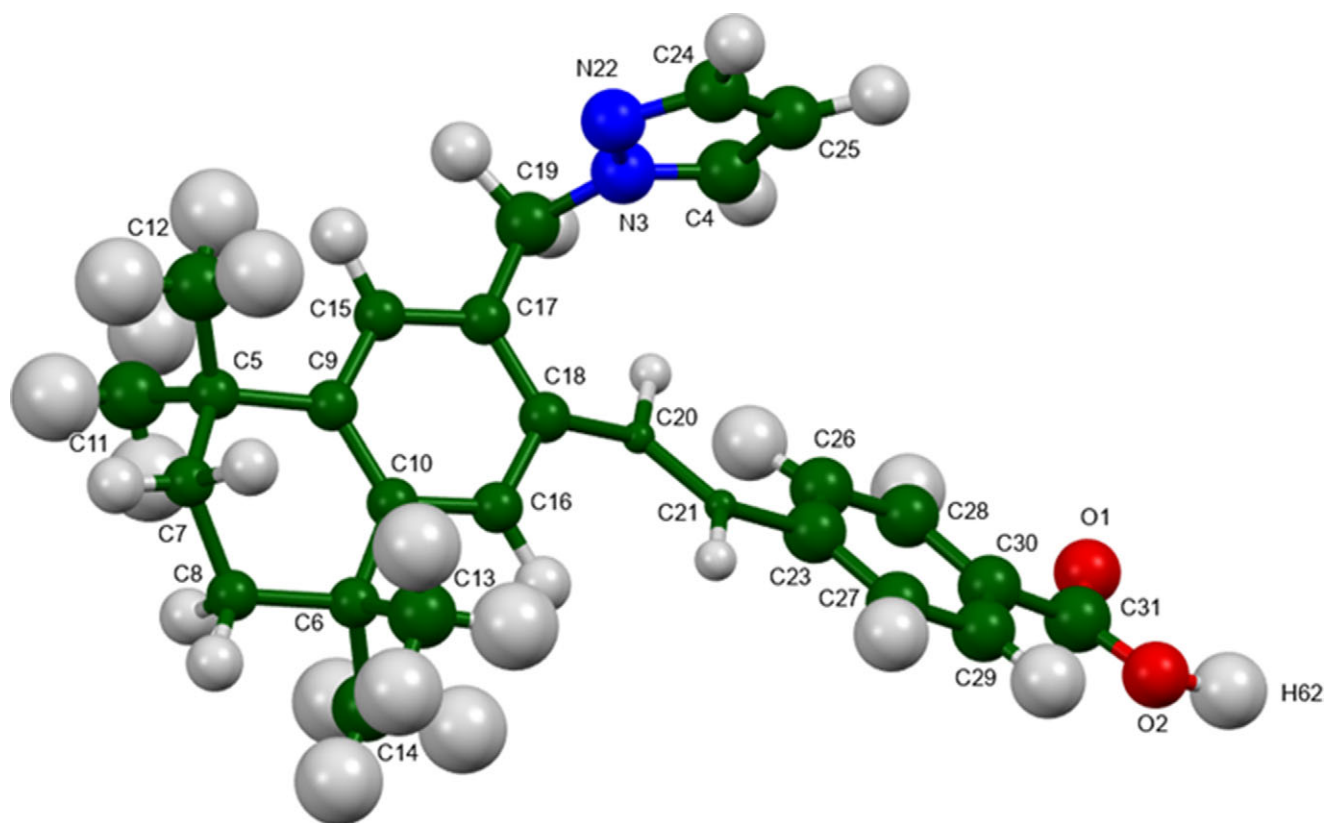
Figure 4. The asymmetric unit of palovarotene, with the atom numbering. The atoms are represented by 50% probability spheroids. Image generated using Mercury (Macrae et al., 2020).
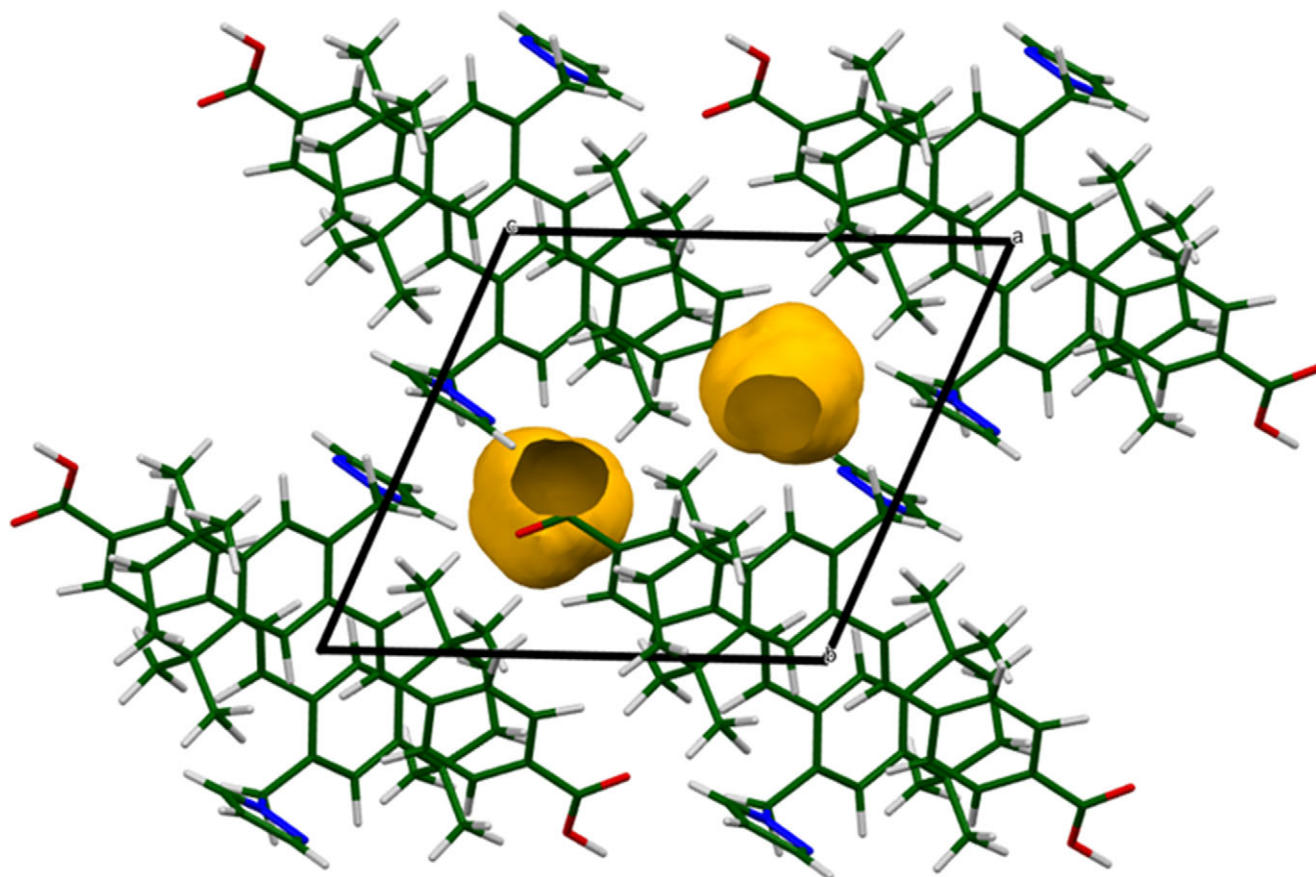

Figure 5. The crystal structure of palovarotene, viewed down the *a*-axis. The yellow surface indicates the void (probe radius = 1.2 Å). Image generated using Mercury (Macrae et al., 2020).

calculation was carried out on 32 cores of a 144-core (768-GB memory) HPE Superdome Flex 280 Linux server at North Central College. The calculation used the GGA-PBE functional, a plane wave cutoff energy of 400.0 eV, and a k-point spacing of 0.5 Å^{-1}, leading to a $2 \times 2 \times 2$ mesh, and took ~2.0 hours. Single-point density functional calculations (fixed experimental cell) and population analysis were carried out using CRYSTAL23 (Erba et al., 2023). The basis sets for the H, C, N, and O atoms in the calculation were those of Gatti et al. (1994). The calculations were run on a 3.5-GHz PC using eight k-points and the B3LYP functional and took ~3.0 hours.

III. RESULTS AND DISCUSSION

The root-mean-square Cartesian displacement of the non-H atoms in the Rietveld-refined and VASP-optimized cations is 0.091 Å (Figure 3). The agreement is within the normal range for correct structures (van de Streek and Neumann, 2014). The asymmetric unit is illustrated in Figure 4. The crystal structure contains a void (Figure 5). Placing an O atom (water molecule) in this void resulted in a refined occupancy of ~0.01, so it was removed from the model. The possibility of hydration/solvation of palovarotene should be remembered. The remaining discussion will emphasize the VASP-optimized structure.

All of the bond distances, bond angles, and torsion angles fall within the normal ranges indicated by a Mercury Mogul Geometry check (Macrae et al., 2020). Quantum chemical geometry optimization of the isolated molecule (DFT/B3LYP/6-31G*/water) using Spartan '24 (Wavefunction, 2023) indicated that the observed solid-state conformation is 4.9 kcal/mol higher in energy than a local minimum, which has a very similar conformation. The global minimum-energy conformation (MMFF force field) is only 0.6 kcal/mol lower in energy but has a different orientation of the pyrazole ring, showing that intermolecular interactions are important to determining the observed conformation.

The crystal structure (Figure 6) consists of chains of hydrogen-bonded palovarotene molecules along the <0,−1,1 > axis. The mean planes of the phenyl, pyrazole, and the aromatic ring of the dihydronaphthalene system are 11, −4, 1; 2, 15, 8; and 6, 3, 5, respectively. The Mercury Aromatics Analyser indicates strong interactions between the phenyl ring and the dihydronaphthalene system (distance = 4.51 Å), and weak dihydronaphthalene–dihydronaphthalene and phenyl–phenyl interactions of 7.56 and 8.47 Å.

Analysis of the contributions to the total crystal energy of the structure using the Forcite module of Materials Studio (Dassault Systèmes, 2023) indicates that angle distortion terms dominate the intramolecular energy, as might be expected for a
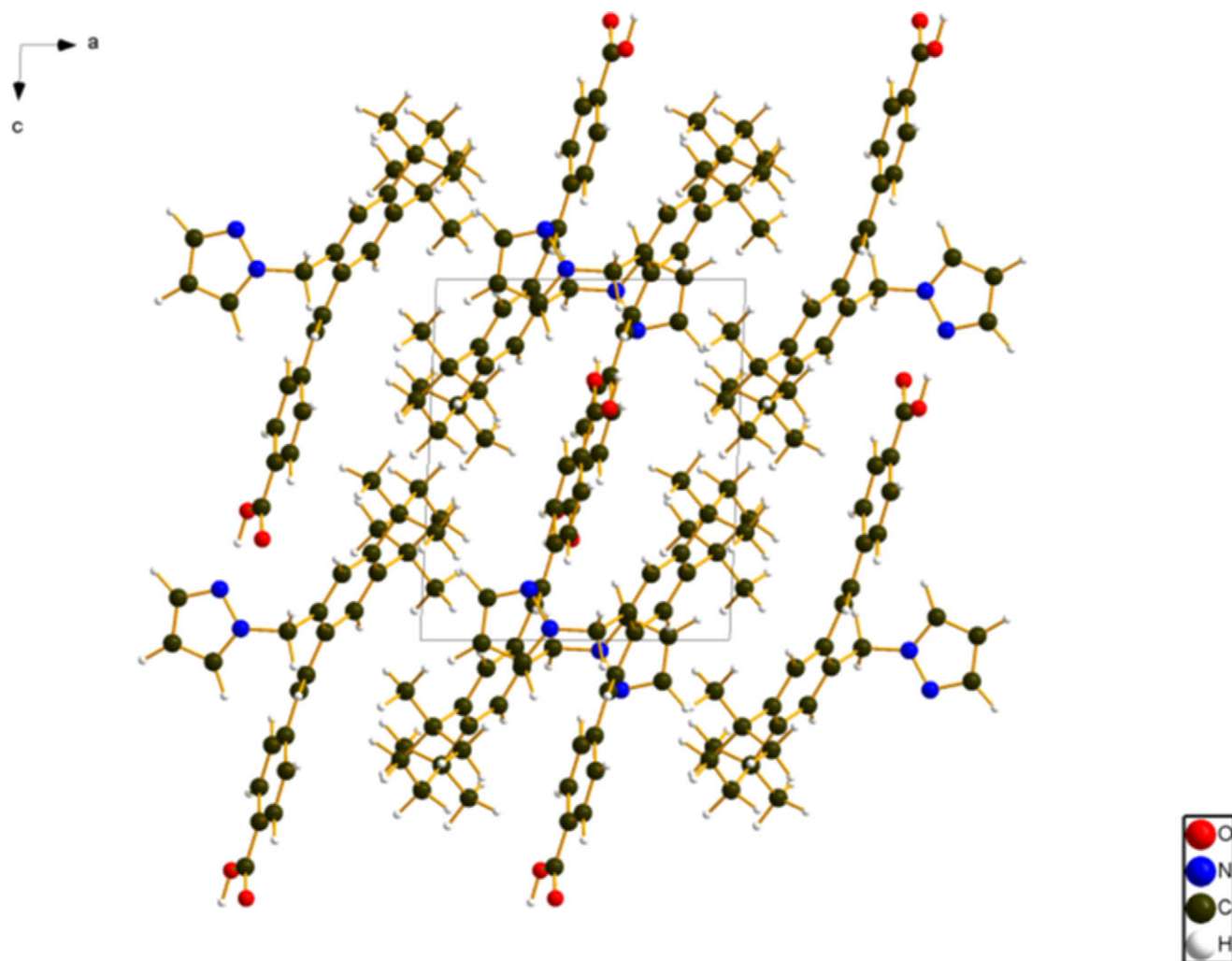

Figure 6. The crystal structure of palovarotene, viewed down the *b*-axis. Image generated using Diamond (Crystal Impact, 2023).

TABLE I. Hydrogen bonds (CRYSTAL23) in palovarotene

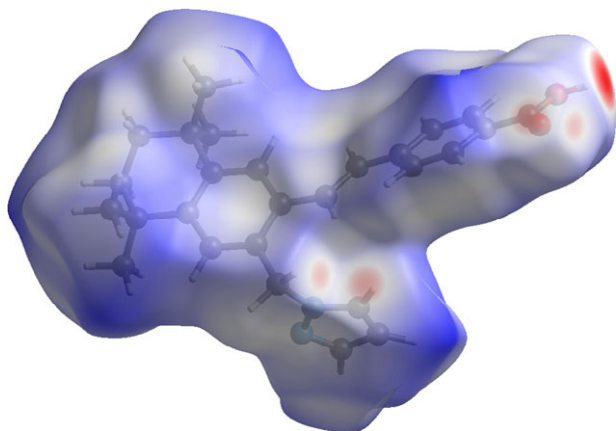| H bond	D–H, Å	H···A, Å	D···A, Å	D–H···A, °	Overlap, e
O2–H62···N22	1.038	1.620	2.650	170.5	0.090
C4–H61···O1	1.086	2.284	3.176	138.0	0.021
C19–H48···O1	1.100	2.384	3.389	151.0	0.019
C29–H57···O2	1.088	2.659	3.482	132.0	0.011
C28–H56···O1	1.090	2.537[a]	2.862	95.9	0.011
C12–H37···O2	1.098	2.610	3.642	156.3	0.011

[a]Intramolecular.

Figure 7. The Hirshfeld surface of palovarotene. Intermolecular contacts longer than the sums of the van der Waals radii are colored blue, and contacts shorter than the sums of the radii are colored red. Contacts equal to the sums of radii are white. Image generated using CrystalExplorer (Spackman et al., 2021).

molecule containing a fused ring system. The intermolecular energy is dominated by electrostatic attractions, which in this force-field-based analysis include hydrogen bonds. The hydrogen bonds are better discussed using the results of the density functional theory (DFT) calculation.

There is only one classical hydrogen bond (Table I). This O2–H62···N22 hydrogen bond links the molecules into chains with a graph set *C1,1(14)* (Etter, 1990; Bernstein et al., 1995; Shields et al., 2000). Several inter- and intramolecular C–H···O hydrogen bonds (to both O atoms of the carboxylic acid group) also contribute to the lattice energy.

The volume enclosed by the Hirshfeld surface of palovarotene (Figure 7; Hirshfeld, 1977; Spackman et al., 2021) is 593.93 Å^3, 98.45% of the unit cell volume. The packing density is thus fairly typical. The only significant close contacts (red in Figure 7) involve the hydrogen bonds. The volume/non-hydrogen atom is larger than normal at 19.4 Å^3.

The Bravais–Friedel–Donnay–Harker (Bravais, 1866; Friedel, 1907; Donnay and Harker, 1937) algorithm suggests that we might expect isotropic morphology for palovarotene. A second-order spherical harmonic model was included in the refinement. The texture index was 1.010(0), indicating that the preferred orientation was not significant in this rotated capillary specimen.

DEPOSITED DATA

The powder pattern of palovarotene from this synchrotron dataset has been submitted to the International Centre for Diffraction Data (ICDD) for inclusion in the Powder Diffraction File. The Crystallographic Information Framework (CIF) files containing the results of the Rietveld refinement (including the raw data) and the DFT geometry optimization were deposited with the ICDD. The data can be requested at pdj@icdd.com.

CONFLICTS OF INTEREST

The authors have no conflicts of interest to declare.

REFERENCES

Altomare, A., C. Cuocci, C. Giacovazzo, A. Moliterni, R. Rizzi, N. Corriero, and A. Falcicchio. 2013. "EXPO2013: A Kit of Tools for Phasing Crystal Structures from Powder Data." *Journal of Applied Crystallography* 46: 1231–35.

Bernstein, J., R. E. Davis, L. Shimoni, and N. L. Chang. 1995. "Patterns in Hydrogen Bonding: Functionality and Graph Set Analysis in Crystals." *Angewandte Chemie International Edition in English* 34: 1555–73.

Black, D. R., D. Windover, A. Henins, J. Filliben, and J. P. Cline. 2011. "Certification of Standard Reference Material 660B." *Powder Diffraction* 26: 155–58.

Bravais, A. 1866. *Etudes Cristallographiques*. Gauthier Villars.

Bruno, I. J., J. C. Cole, M. Kessler, J. Luo, W. D. S. Motherwell, L. H. Purkis, B. R. Smith, et al. 2004. "Retrieval of Crystallographically Derived Molecular Geometry Information." *Journal of Chemical Information and Computer Sciences* 44: 2133–44.

Crystal Impact. 2023. *Diamond V. 5.0.0*. Crystal Impact – Dr. H. Putz & Dr. K. Brandenburg.

Dassault Systèmes. 2023. *BIOVIA Materials Studio 2024*. BIOVIA.

Donnay, J. D. H., and D. Harker. 1937. "A New Law of Crystal Morphology Extending the Law of Bravais." *American Mineralogist.* 22: 446–47.

Erba, A., J. K. Desmarais, S. Casassa, B. Civalleri, L. Donà, I. J. Bush, B. Searle, et al. 2023. "CRYSTAL23: A Program for Computational Solid State Physics and Chemistry." *Journal of Chemical Theory and Computation* 19: 6891–932. https://doi.org/10.1021/acs.jctc.2c00958.

Etter, M. C. 1990. "Encoding and Decoding Hydrogen-Bond Patterns of Organic Compounds." *Accounts of Chemical Research* 23: 120–26.

Favre-Nicolin, V., and R. Černý. 2002. "FOX, 'Free Objects for Crystallography': A Modular Approach to Ab Initio Structure Determination from Powder Diffraction." *Journal of Applied Crystallography* 35: 734–43.

Friedel, G. 1907. "Etudes sur la loi de Bravais." *Bulletin de la Société Française de Minéralogie* 30: 326–455.

Gatti, C., V. R. Saunders, and C. Roetti. 1994. "Crystal-Field Effects on the Topological Properties of the Electron-Density in Molecular Crystals – the Case of Urea." *Journal of Chemical Physics* 101: 10686–96.

Groom, C. R., I. J. Bruno, M. P. Lightfoot, and S. C. Ward. 2016. "The Cambridge Structural Database." *Acta Crystallographica Section B: Structural Science, Crystal Engineering and Materials* 72: 171–79.

Hirshfeld, F. L. 1977. "Bonded-Atom Fragments for Describing Molecular Charge Densities." *Theoretica Chemica Acta* 44: 129–38.

Kabekkodu, S., A. Dosen, and T. N. Blanton. 2024. "PDF-5+: A Comprehensive Powder Diffraction File™ for Materials Characterization." *Powder Diffraction* 39: 47–59.

Kaduk, J. A., C. E. Crowder, K. Zhong, T. G. Fawcett, and M. R. Suchomel. 2014. "Crystal Structure of Atomoxetine Hydrochloride (Strattera), $C_{17}H_{22}NOCl$." *Powder Diffraction* 29: 269–73.

Kim S., J. Chen, T. Cheng, A. Gindulyte, J. He, S. He, Q. Li, B. A. Shoemaker, et al. 2023. "PubChem 2023 Update." *Nucleic Acids Research* 51 (D1): D1373–80. https://doi.org/10.1093/nar/gkac956.

Kresse, G., and J. Furthmüller. 1996. "Efficiency of Ab-Initio Total Energy Calculations for Metals and Semiconductors Using a Plane-Wave Basis Set." *Computational Materials Science* 6: 15–50.

Leontowich, A. F. G., A. Gomez, B. Diaz Moreno, D. Muir, D. Spasyuk, G. King, J. W. Reid, C.-Y. Kim, and S. Kycia. 2021. "The Lower Energy Diffraction and Scattering Side-Bounce Beamline for Materials Science at the Canadian Light Source." *Journal of Synchrotron Radiation* 28: 1–9. https://doi.org/10.1107/S1600577521002496.

Leslie, M. 2024. "Drug Development Blossoms for Rare, Fatal Bone Disease." *Science* 384: 943–44.

Macrae, C. F., I. Sovago, S. J. Cottrell, P. T. A. Galek, P. McCabe, E. Pidcock, M. Platings, et al. 2020. "*Mercury 4.0*: From Visualization to Design and Prediction." *Journal of Applied Crystallography* 53: 226–35.

Materials Design. 2024. *MedeA 3.7.2*. Materials Design, Inc.

O'Boyle, N. M., M. Banck, C. A. James, C. Morley, T. Vandermeersch, and G. R. Hutchison. 2011. "Open Babel: An Open Chemical Toolbox." *Journal of Chemical Informatics* 3: 33. https://doi.org/10.1186/1758-2946-3-33.

Shields, G. P., P. R. Raithby, F. H. Allen, and W. D. S. Motherwell. 2000. "The Assignment and Validation of Metal Oxidation States in the Cambridge Structural Database." *Acta Crystallographica Section B: Structural Science* 56: 455–65.

Spackman, P. R., M. J. Turner, J. J. McKinnon, S. K. Wolff, D. J. Grimwood, D. Jayatilaka, and M. A. Spackman. 2021. "CrystalExplorer: A Program for Hirshfeld Surface Analysis, Visualization and Quantitative Analysis of Molecular Crystals." *Journal of Applied Crystallography* 54: 1006–11. https://doi.org/10.1107/S1600576721002910; https://crystalexplorer.scb.uwa.edu.au.

Stephens, P. W. 1999. "Phenomenological Model of Anisotropic Peak Broadening in Powder Diffraction." *Journal of Applied Crystallography* 32: 281–89.

Sykes, R. A., P. McCabe, F. H. Allen, G. M. Battle, I. J. Bruno, and P. A. Wood. 2011. "New Software for Statistical Analysis of Cambridge Structural Database Data." *Journal of Applied Crystallography* 44: 882–86.

Toby, B. H., and R. B. Von Dreele. 2013. "GSAS II: The Genesis of a Modern Open Source All Purpose Crystallography Software Package." *Journal of Applied Crystallography* 46: 544–49.

van de Streek, J., and M. A. Neumann. 2014. "Validation of Molecular Crystal Structures from Powder Diffraction Data with Dispersion-Corrected Density Functional Theory (DFT-D)." *Acta Crystallographica Section B: Structural Science, Crystal Engineering and Materials* 70: 1020–32.

Wavefunction, Inc. 2023. *Spartan '24. V. 1.0.0*. Wavefunction, Inc.